Numerical survey of predicted peeling response in ELM mitigated and suppressed phases on ASDEX Upgrade

D A Ryan[1], M Dunne[2], A Kirk[1], S Saarelma[1], W Suttrop[2], C Ham[1], Y Q Liu[3], M Willensdorfer[2], the ASDEX Upgrade team[2] and the MST1 team[1]

[1] CCFE, Culham Science Centre, Abingdon, Oxfordshire, UK

[2] Max Planck Institute for Plasma Physics, Garching, Germany

[3] General Atomics, P. O. Box 85608, San Diego, California 92186-5608, USA

Abstract. Using the MARS-F linear MHD code (Liu *et al* 2000 *Phys. Plasmas* **7** 3681), a numerical survey of the plasma response to applied RMPs in ASDEX Upgrade ELM control experiments is conducted, to clarify the role of triangularity and the peeling response in the suppression mechanism. The peeling response is found to decrease with increasing triangularity, due to an increase in the coil-plasma gap reducing the effective vacuum field. Therefore the prior hypothesis that the requirement of high triangularity for suppression access is due to the requirement of a sufficiently large peeling response[2] is suspected to be incorrect. A secondary hypothesis is proposed, that in high triangularity the drive of the resonant response by the peeling response may be boosted by enhanced poloidal harmonic coupling, which could explain the requirement of high triangularity for suppression access. It is shown that in fact the poloidal harmonic coupling between the resonant and off-resonant components decreases with triangularity, and therefore this hypothesis is also rejected. Finally an alternative hypothesis is discussed, that high triangularity is required to access suppression because the associated enhanced pedestal stability allows the edge deformation to be large enough to control the density, without the reduction in stability due to boundary deformation destabilising ELMs. A rigorous test of this hypothesis requires models to be developed to compute the stability of experimental 3D equilibria.

1. Introduction

The ITER tokamak is expected to operate primarily in an ELM-y H-mode regime, which features a quasi-periodic MHD instability known as the Edge Localised Mode (ELM). ELMs are triggered when the edge pedestal exceeds a stability threshold in pressure gradient or current[3]. This causes a dramatic collapse in the pedestal pressure, and subsequently a short transient of high heat flux to impact the plasma facing components, which is expected to exceed the material damage limit of the ITER divertor if left unmitigated[4]. Fortunately, it has been demonstrated that the application of Resonant Magnetic Perturbations (RMPs) may prevent ELMs from being triggered, while retaining stable H-mode operation, a regime referred to as ELM suppression[5]. ELM suppression has now been reproduced on many major tokamaks currently operating[5, 6, 7, 8], however the suppressed regime is accessible only in certain small regions of parameter space[9], and the access conditions are not known comprehensively. In contrast, ELM mitigation is a far more readily accessible regime[9], in which the RMPs cause the ELMs to trigger at a faster rate, which reduces the energy content and peak heat flux of individual ELMs[10]. Given these promising results, a flexible set of RMP coils has been added to the ITER design[11], and intensive research efforts are focussed on developing robust and predictive theories of ELM mitigation and suppression, in order to assess and optimise the ITER ELM control strategy.

Besides modifying the ELM frequency, the application of RMPs has many other observable effects on tokamak plasmas, which may provide clues as to the physical mechanisms of mitigation and suppression. RMPs are commonly observed to cause a decrease in the plasma particle density, referred to as density pump out, and a braking of the plasma rotation[6]. Also, applying RMPs to a 2D plasma equilibrium causes measurable 3D deformation of the plasma flux surfaces[12, 13], colloquially known as corrugation[14, 15]. The resulting 3D equilibrium has reduced P-B stability relative to the unperturbed 2D equilibrium, which is suspected to be the driving mechanism for ELM mitigation[16, 17, 18, 19]. Furthermore, if the component of the RMP aligned to the equilibrium magnetic field, commonly referred to as the resonant field or pitch aligned field, is finite, then magnetic island chains may form in the plasma. Strong experimental and modelling evidence[20, 21], suggests that suppression may be achieved when the electron perpendicular flow vanishes near a rational surface, allowing an island chain to form near the pedestal top which restricts the expansion of the pedestal width, restraining the plasma pedestal within the stable region.

However, the applied vacuum field is drastically altered by the response of the plasma, and neither the plasma corrugation, nor the extent of island formation may be accurately predicted without accounting for this response [22, 23, 24]. The plasma response typically manifests as a strong screening of the resonant field, and also the amplification of marginally stable MHD modes in the plasma bulk. A particular class of these stable modes are of interest to working theories of ELM control, localised to the plasma edge with poloidal mode numbers

just above resonance, commonly referred to as the peeling response[25]. The peeling response has numerous roles in ELM control theories and the experimental evidence base. Firstly, it is predicted theoretically that the amplified peeling response may drive the resonant field via poloidal harmonic coupling[25], which may facilitate island formation. Secondly, the corrugation which is predicted to degrade P-B stability, is amplified by the peeling response. Thirdly, it is observed that when the applied field is tuned to maximally amplify the peeling response, the mitigated ELM frequency and density pump out are also maximised[26], and the coil current threshold for ELM suppression access is minimised[23, 8, 6]. The correlation between the peeling response and ELM frequency may be caused by the deleterious effect of increasing edge corrugation on P-B stability, while the correlation with suppression access may be due to the role of the peeling response in driving the resonant field, or perhaps in controlling the density via density pump out. It seems that the peeling response may have a crucial role in determining both the transport and stability properties of RMP perturbed plasmas, which must be further clarified.

Recent experimental campaigns on ASDEX Upgrade have achieved complete ELM suppression, demonstrating that tuning the applied field to optimally amplify the peeling response, and achieving a sufficiently high upper triangularity δ_U, are crucial suppression access parameters. It is proposed in [2], that increasing δ_U allows access to higher pedestal pressures, which boosts the peeling response and thereby facilitates suppression access. In this work, the role of δ_U and the peeling response in achieving ELM suppression is investigated using a numerical survey of the plasma response in experimental conditions. In section 2, a database of ASDEX Upgrade ELM control experiments is described, metrics used to characterise the plasma response are explained and compared, and pedestal properties which may affect the peeling response are examined. In section 3, the plasma response to experimentally applied RMP fields is computed using the MARS-F linear MHD code, using the database points as model input. It is shown that in experiments, increasing δ_U moves the plasma boundary away from the RMP coils, reducing the effective vacuum field inside the plasma and consequently the peeling response. This effect dominates over the meagre increase in peeling response due to increased pedestal pressure, resulting in a net decrease of the peeling response with triangularity. This implies that the hypothesis described previously for explaining the high δ_U requirement[2], is likely to be incorrect.

In section 4, an alternative hypothesis is proposed, that the requirement of high triangularity may be a consequence of increased triangularity induced $\Delta m = 3$ poloidal harmonic coupling (PHC). Increasing $\Delta m = 3$ PHC may allow the peeling response to drive the resonant field more efficiently, increasing the resonant field for a fixed peeling response and facilitating island formation. This suggestion is tested with a numerical scan of the upper triangularity, and with the survey. It is found that while triangularity induced PHC does increase with δ_U as expected, it is more than compensated by a decrease in toroidicity induced $\Delta m = 1$ coupling. The result is that the drive of the resonant components by PHC is found to decrease with δ_U, so this explanation for the high triangularity requirement for suppression is also rejected.

Finally, in section 5 an alternative explanation of the requirement for high triangularity is described, to be tested in future works. Following [16], it is explained that edge corrugation driven by the peeling response degrades P-B stability. A reduction of the P-B stability limit may compensate for movement of the operational point towards the stable region as the peeling response and density pump out increase, keeping the operational point P-B unstable. In principle, the enhanced P-B stability of high triangularity plasmas would increase their resilience to corrugation induced destabilisation, which may explain the requirement of high triangularity for suppression access.

2. ASDEX Upgrade ELM Control Database

Numerous RMP ELM control campaigns on ASDEX Upgrade have recently been conducted, adding many examples of both mitigation and suppression[2, 27] to the experimental archive. In this section, the assembled database of points from selected ASDEX Upgrade ELM control experiments is described. Points are chosen from both high and low δ_U RMP ELM control experiments in which either suppression or mitigation was achieved, avoiding close temporal proximity to transitions into or out of suppression. For mitigated phases, the ELM frequency at each point is extracted and included in the database. Quantifying the extent of mitigation relative to the natural ELM frequency is beyond the scope of this study, so for simplicity this work will define 'good' mitigation as $f_{ELM} > 200$, and 'poor' mitigation as $f_{ELM} < 200$. For each chosen point, an mtanh function[28] is fitted to experimental measurements of T_e, T_i, n_e, and a spline to toroidal bulk rotation velocity v_T, with a 20ms integration time. When appropriate, a radial shift is applied to the T_e data measured using the edge Thompson scattering diagnostic, to enforce $T_e \approx 100eV$ at the separatrix. To ensure consistency between the T_e and n_e profiles, this same shift was then applied to the density profile as measured using the same diagnostic, as performed in [29]. An ELM synchronisation technique is commonly used for measuring pedestal profiles of ELM-y plasmas[29], in order to isolate the pedestal profile immediately preceding the ELM crash. However, for this work measurements of the ion temperature and rotation velocity by the CXRS diagnostic were required[30], which has a time resolution comparable to the ELM frequencies of interest to this study, making ELM synchronisation infeasible. The measured pedestal heights and gradients are therefore expected to be slightly lower than the saturated phase of the ELM cycle, however this effect is mitigated by the high frequency and corresponding small size of the ELMs studied here. An equilibrium reconstruction is then manually performed for each point using the CLISTE[31] equilibrium code, constrained by magnetic measurements integrated over the same period as the kinetic profiles, and using the measured kinetic profiles to constrain the edge pressure profile. The experimentally applied RMP coil currents are extracted from the experimental archive, and corrections for the field attenuation due to eddy currents in the passive stability loops (PSLs) are computed using a finite element modelling code[32] as in previous studies[26], and applied as scaling factors in post processing. Using this data as model input, the plasma response to the applied field is then computed using the extensively

percentile	q_{95}	β_N	$n_{e,0}$ (m^{-3})	$t_{e,0}$ (keV)	R_0 (m)	B_0 (T)	I_p (MA)
10th	3.84	1.12	3.67×10^{19}	3.05	1.675	1.795	0.748
25th	3.92	1.64	4.38×10^{19}	3.65	1.679	1.806	0.773
50th	4.02	1.80	5.25×10^{19}	4.53	1.687	1.820	0.814
75th	4.11	2.03	6.01×10^{19}	5.41	1.695	1.831	0.829
90th	4.22	2.27	6.64×10^{19}	6.09	1.701	1.841	0.841

Table 1. Summary of the spread of plasma parameters in the database.

benchmarked and validated [33, 34, 13] linear MHD code MARS-F [35], and the peeling response quantified using metrics described below. The essential plasma parameters in the database are summarised in table 1. Injected density and NBI power are tightly clustered around $0.92\times10^{21}m^{-3}s^{-1}$ and 6 MW respectively, with a few outliers. So that the effect of varying δ_U may be examined, points were taken from low and high δ_U experiments. In this study, 'high' triangularity denotes $\delta_U > 0.18$, while 'low' triangularity denotes $\delta_U < 0.18$. In this database, plasma shapes with higher δ_U tended also to have lower elongation, and the lower triangularity δ_L was also marginally higher.

## 2.1. Peeling response scalar metrics

In previous studies it has been shown that ELM control observations are strongly correlated with certain metrics derived from the plasma response, the most widely used of which are the outermost resonant component of the total magnetic perturbation $|b^1_{res}|$ (correlated with ELM frequency[19]), and the normal displacement of the plasma surface around the X point $|\xi_n X(s=1)|$ (correlated with density pump out[36]). These metrics are suitable for studies of a single plasma equilibrium, or for coil optimisation studies for which they have been used in the past[26, 37]. The MARS-F code cannot resolve the plasma X point, so in MARS-F studies the plasma boundary is distorted to smooth out the X point. In the aforementioned studies, the dependence of the metrics on the coil phase difference was the crucial quantity, which is robust to the degree of boundary distortion required to truncate the X point. However the absolute values of $|b^1_{res}|$ and $|\xi_n X(s=1)|$ as previously used are not strictly robust to X point truncation, and so are unsuitable for comparison between different equilibria which this study is concerned with. In this work, simplified metrics are chosen to capture the edge peeling plasma response while being robust to truncation. Bulk magnetic metrics $b_n\{T/X\}\{tot/resp\}$ refer to the total (tot) or pure response ($resp$) magnetic field normal to flux surfaces maximised over the plasma top (T) or X point (X) regions. The regions over which the magnetic field is maximised are sketched in Figure 1. We distinguish between the total magnetic field and pure response (ie, total - vacuum field) since the former is indicative of the 'real' field which may be measured in experiments, while the latter more closely corresponds to the peeling response since it does not contain the vacuum field. Since the edge peeling response commonly manifests in the ($m = nq + 2, 3$) spectral region, a spectral
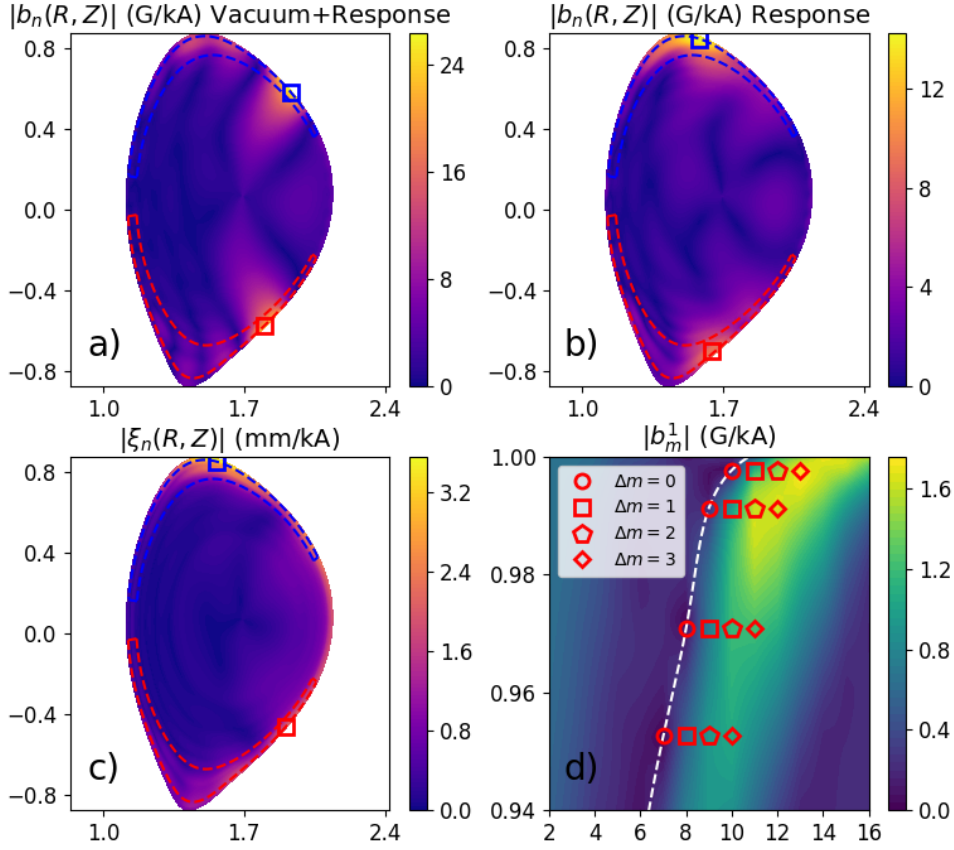
Figure 1. Explanations of the metrics used here to quantify the plasma response. a) $b_n T_{tot}$ and $b_n X_{tot}$ are the total magnetic perturbation (sum of vacuum field and plasma response) maximised over the regions outlined above, near the plasma top and plasma X point. The squares denote the location of maximal total field for this example, where $b_n T_{tot}$ and $b_n X_{tot}$ are measured. b) $b_n T_{resp}$ and $b_n X_{resp}$ are the magnetic plasma response (total - vacuum) maximised over the same regions. c) $\xi_n T$ and $\xi_n X$ are the plasma displacement normal to flux surfaces, maximised over the same regions. d) Spectral magnetic metrics $b^1_{m=nq+\Delta m}$ refer to the outermost off resonant components of the total magnetic perturbation, normal to flux surfaces.

magnetic metric $b^1_{m=nq+\Delta m}$ for $\Delta m = 1, 2, 3$ is used, referring to the outermost 'off-resonant' components of the total magnetic field. Displacement metrics $\xi_n\{T/X\}$ refer to the plasma displacement normal to flux surfaces, maximised over the plasma top (T) or X point (X) regions.

For each point in the database, the plasma response to a fixed static 1kA (5kAt) field with a fixed coil phase difference $\Delta\phi_{ul} = 90$ degrees is computed with MARS-F (in later sections, the experimental coil currents are used, and corrections for field attenuation due to eddy currents in the passive stabilisation loops are included). The poloidal coordinate is resolved
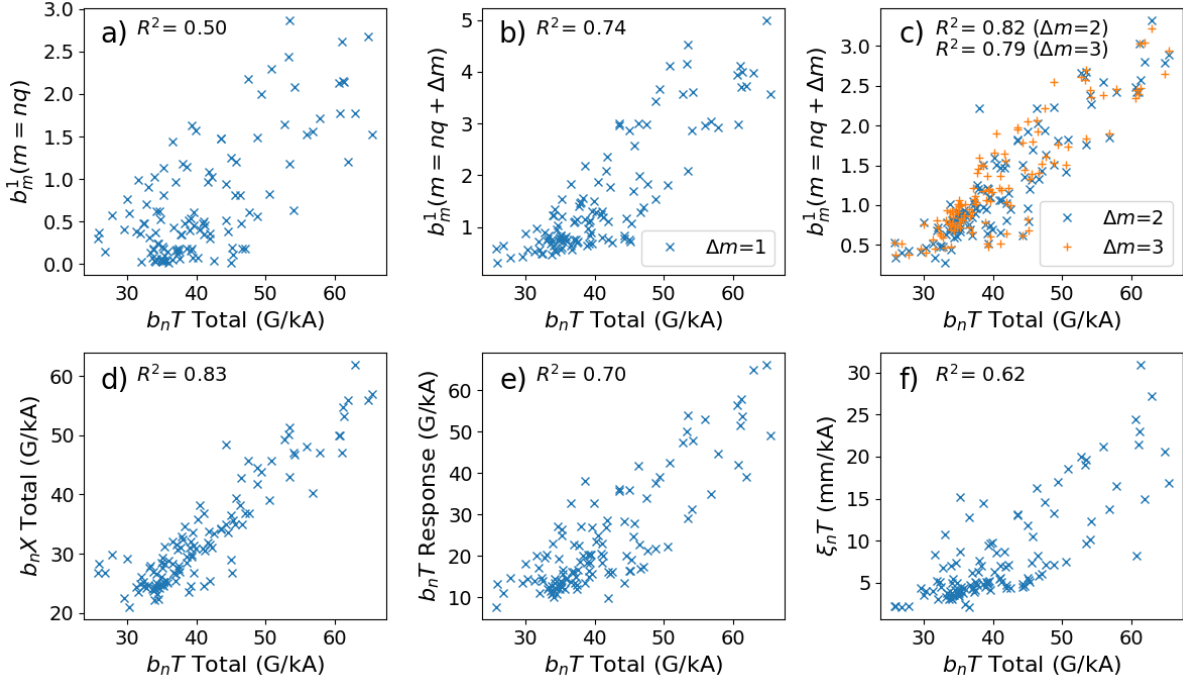
Figure 2. For each point in the database, the plasma response to a fixed static 1kA (5kAt) field with a fixed coil phase difference $\Delta\phi_{ul} = 90$ degrees is computed with MARS-F, and scalar metrics extracted. a) Outermost resonant component plotted against $b_n T_{tot}$. b,c) Outermost off resonant components plotted against $b_n T_{tot}$. d) $b_n X_{tot}$ plotted against $b_n T_{tot}$. e) $b_n T_{resp}$ plotted against $b_n T_{tot}$. f) $\xi_n T$ plotted against $b_n T_{tot}$.

with 60 poloidal Fourier harmonics, and the radial coordinate is resolved with 480 radial mesh points within the plasma with dense packing at rational surfaces, and 180 mesh points to resolve the vacuum region. For each database point, the X point region of the plasma boundary is smoothed manually, rather than using flux truncation, in order to preserve the plasma boundary shape away from the X point. Parallel viscosity is modelled in MARS-F using a viscous sound wave damping model, which requires a numerical parameter to determine the strength of the damping[38]. In this work the chosen value of the parallel sound wave damping coefficient was 1.5, corresponding to strong parallel sound wave damping[22]. It is previously observed that magnetic and displacement metrics and their corresponding experimental observables, have similar dependencies on the coil phase difference $\Delta\phi_{ul}$[39, 40, 26]. It is also expected that this set of metrics will be correlated with each other even for fixed $\Delta\phi_{ul}$ and applied field, and therefore one metric may be used as a proxy for the others. Figure 2 plots the peeling response metrics against the total magnetic perturbation in the plasma top region $b_n T_{tot}$, using a constant applied field amplitude of $1kA$ ($5kAt$) with a fixed coil phase difference $\Delta\phi_{ul} = 90$ degrees. Figure 2a) plots $b_n T_{tot}$ against the outermost resonant component $b^1_{m=nq}$. Although the applied field is constant, a correlation is apparent between the resonant component and $b_n T_{tot}$. This is consistent with previous predictions[25] that the resonant field may be driven by the edge peeling response via poloidal harmonic coupling. However, numerical truncation of the plasma X point modifies the edge safety factor profile,

causing the location of the outermost resonant component to move relative to the resistivity and rotation profiles. This introduces a potentially large uncertainty into the absolute value of $b_{m=nq}^1$, and it is therefore not used as a metric for the peeling response in this study. Figures 2b) and c) plot $b_n T_{tot}$ against the off-resonant components $b_{m=nq+\Delta m}^1$ for $\Delta m = 1, 2, 3$. The strong correlations apparent suggest that the peeling response may be assessed either using the spectral or bulk metrics. It is also consistent with the common observation that the peeling response manifests primarily in the spectral region of $m = nq + \Delta m$ for $\Delta m = 1, 2, 3$. Figure 2d) plots $b_n X_{tot}$ against $b_n T_{tot}$. The strong correlation ($R^2 = 0.83$) indicates that the peeling response may be measured either at the plasma top or bottom without significantly affecting the results. This is useful since we may characterise the peeling response at both the plasma top and X point regions using a single scalar. Since changing the upper triangularity δ_U more strongly affects the upper geometry than lower, it is intuitively expected that varying δ_U would more directly affect the response in the upper plasma region than the lower. Therefore this work will primarily use metrics defined in the upper plasma region (ie, $b_n T_{tot}$). Figure 2e) plots $b_n T_{tot}$ against $b_n T_{resp}$. Correlation is trivially expected since the total field is the sum of the vacuum field and response, and also because the plasma response is an amplification of the vacuum field and is therefore proportional to it. However the correlation is somewhat confounded since the two metrics are measured at different locations in the poloidal plane, as demonstrated by Figures 1a,b). In the majority of cases, the total magnetic field at the plasma edge is dominated by the vacuum field, and so the maximum where $b_n T_{tot}$ is measured is found at the point closest to the coils (for consistency, points where this is not the case are excluded), while the maximum of the plasma response where $b_n T_{resp}$ is measured tends to be in a region of low B_p, ie, at the plasma top. Figure 2f) plots $b_n T_{tot}$ against the maximum displacement in the plasma top region $\xi_n T$, demonstrating the correlation between plasma displacement and total field previously observed for scans of coil phase $\Delta\phi_{ul}$. The metrics chosen are highly correlated with each other, so the precise choice of whether to characterise the plasma response using the X point or plasma top region, total magnetic field, pure response field or displacement, has limited significance.

2.2. Pressure dependence on δ_U

The hypothesis outlined in [2] for the high δ_U requirement for suppression proposes that the pedestal pressure increases with δ_U, in order to boost the pressure drive for the peeling response, primarily via an increase in the pressure gradient driven bootstrap current. Figure 3 plots the equilibrium pressure at the pressure pedestal and s=0.99, against upper triangularity δ_U for the dataset points. Radial coordinate s is defined as $s = \sqrt{\psi_N} = \sqrt{\frac{\psi_{pol}-\psi_0}{\psi_a-\psi_0}}$, where ψ_{pol} and ψ_N are the poloidal flux and normalised poloidal flux respectively, and ψ_0 and ψ_a are the poloidal flux at the magnetic axis and plasma edge respectively. Since the equilibrium pressure profile is derived from the solution of the Grad-Shrafanov equation constrained by experimental measurements, the pedestal is not guaranteed to be an mtanh shape. Therefore in this work, the pedestal is defined to be located at the minimum of the

second derivative of the pressure profile, where the decrease in the pressure gradient is the largest (ie, $\min[\partial^2 P_{EQ}/\partial s^2]$). The database also contains points from an experimental scan of δ_U in discharge 34835, which is also plotted in the figure. To reduce the input power as a confounding variable, a filter is applied to restrict β_N to within $1.7 < \beta_N < 2.1$ (the points from the 34835 scan are not subject to this constraint). An increase in the pedestal pressure with δ_U is expected, consistent with [29]. The plots do not refute this, but the scatter is large enough that they provide only weak evidence in support of it. The effect of triangularity on pedestal pressure is well documented[29], suggesting that confounding factors are obscuring the trend in this result.
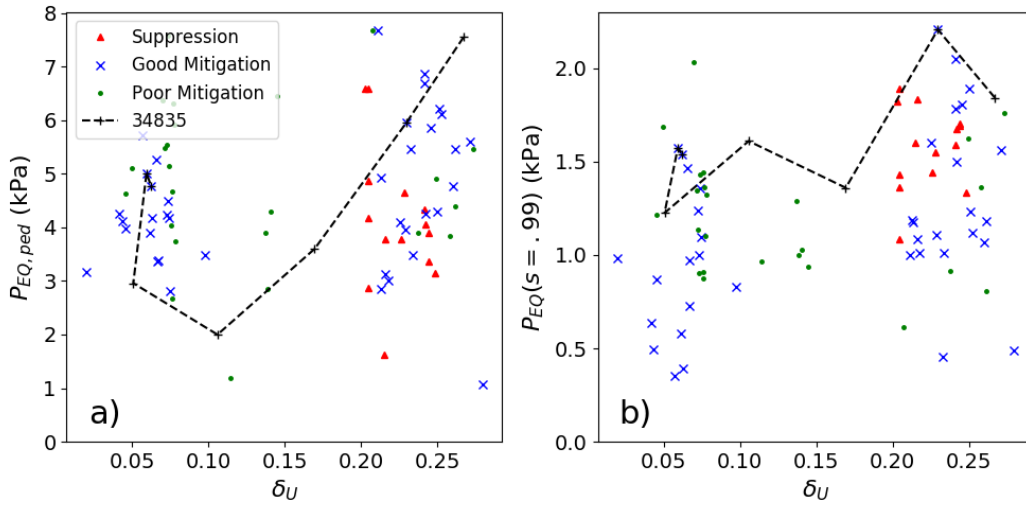

Figure 3. a) Equilibrium pedestal pressure against plasma triangularity. b) Equilibrium plasma pressure at the $s = \sqrt{\psi_N} = 0.99$ surface against plasma triangularity. In both subplots, β_N is restricted to within $1.7 < \beta_N < 2.1$. The δ_U scan of discharge 34835 is not subject to this constraint. The pedestal top locations of these data are quite tightly clustered, with a mean and standard deviation of $s = 0.969 \pm 0.013$. During the δ_U scan of discharge 34835, the power and fueling are constant, and β_N varies in the scan from 1.5 to 2.1 directly proportional to the equilibrium pedestal pressure. The scatter is too large to conclude from the database that a correlation exists between pedestal pressure and δ_U.

2.3. Pressure dependence on density

It is established experimentally that suppression access requires the density to be reduced below some critical value[6]. This implies that the pedestal pressure, dominated by the thermal pressure, will be reduced in suppressed relative to mitigated cases. This would imply a lower pressure drive for the peeling response, and may lead to the peeling response being systematically lower in the suppressed cases relative to mitigated. Figure 4a) plots the thermal plasma pressure (neglecting Z_{eff}) against electron number density at the thermal plasma pressure pedestal (located in the same way as the equilibrium pressure pedestal), for the high triangularity points only ($0.18 < \delta_U < 0.28$). It appears that the edge density of

the suppression discharges being capped at around $3 \times 10^{19} m^{-3}$, does result in the pedestal pressure being systematically lower in suppression than mitigation. Figure b) plots the sum of $T_i + T_e$ against n_e at the thermal plasma pressure pedestal, for the same points (also neglecting Z_{eff}). The figure indicates that the loss of density in the suppression phase is not compensated by higher particle temperatures, resulting in a lower pedestal pressure. This result leads us to expect slightly reduced pressure drive of the peeling response between the suppressed and mitigated phases for fixed triangularity.
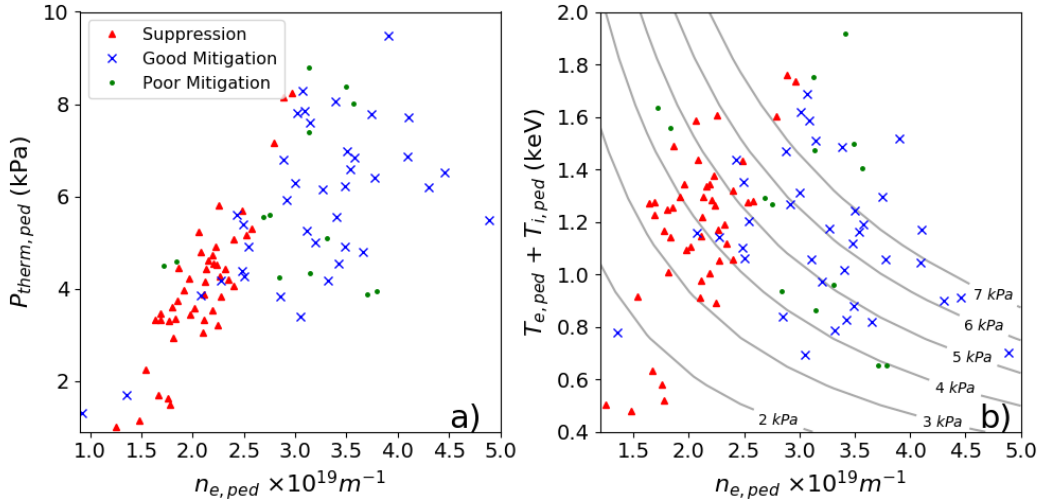

Figure 4. a) The thermal plasma pressure $P_{therm,ped}$, plotted against electron number density, both evaluated at the thermal plasma pedestal. b) Sum of the ion and electron temperatures plotted against electron number density, both evaluated at the thermal plasma pedestal.

3. Peeling response in mitigation and suppression, and δ_U dependence

For each point in the database described previously, the plasma response to the experimentally applied RMP field is computed with MARS-F, and corrected for PSL attenuation. Figure 5a) plots the total bulk magnetic field $b_n T_{tot}$ against the $\Delta m = 1$ off resonant component of the total field, $b^1_{m=nq+1}$, for cases of mitigation and suppression. Figure 5c) plots the pure magnetic plasma response $b_n T_{resp}$ against the normal plasma displacement $\xi_n T$. The metrics $b_n T_{tot}$ and $b^1_{m=nq+1}$ used in figure a) include the vacuum field, meaning that they represent the field which physically exists in experiments and may in principle be measured. However, the vacuum field may confound measurement of the pure plasma response. Metrics $b_n T_{resp}$ and $\xi_n T$ used in figure c) are more directly indicative of the plasma response. All model input used to compute the points in figures 5a,c) were derived from experimental machine parameters and experimental measurement. Therefore, we may expect the results plotted in figures a,c) to represent a survey of the peeling response which occurred in the recent ASDEX Upgrade ELM control experimental campaigns. The mean and spread (simple standard deviation) of the mitigation and suppression points separately are also plotted. While the data from

the suppression and mitigation sets overlap to a large degree and there is no clear threshold between the states, the averages for each set indicate that, considering the database as a whole, the peeling response tends to be lower in suppression than mitigation in this dataset. Figures 5b,d) plot these same metrics, but with a fixed applied field of 1kA (5kAt) and coil phase $\phi_{ul} = 90$, removing all variation in the applied field as in figure 2. The shift to lower peeling response in suppression is still evident in this plot, indicating that it is due to equilibrium variations between the two phases rather than applied field variations.
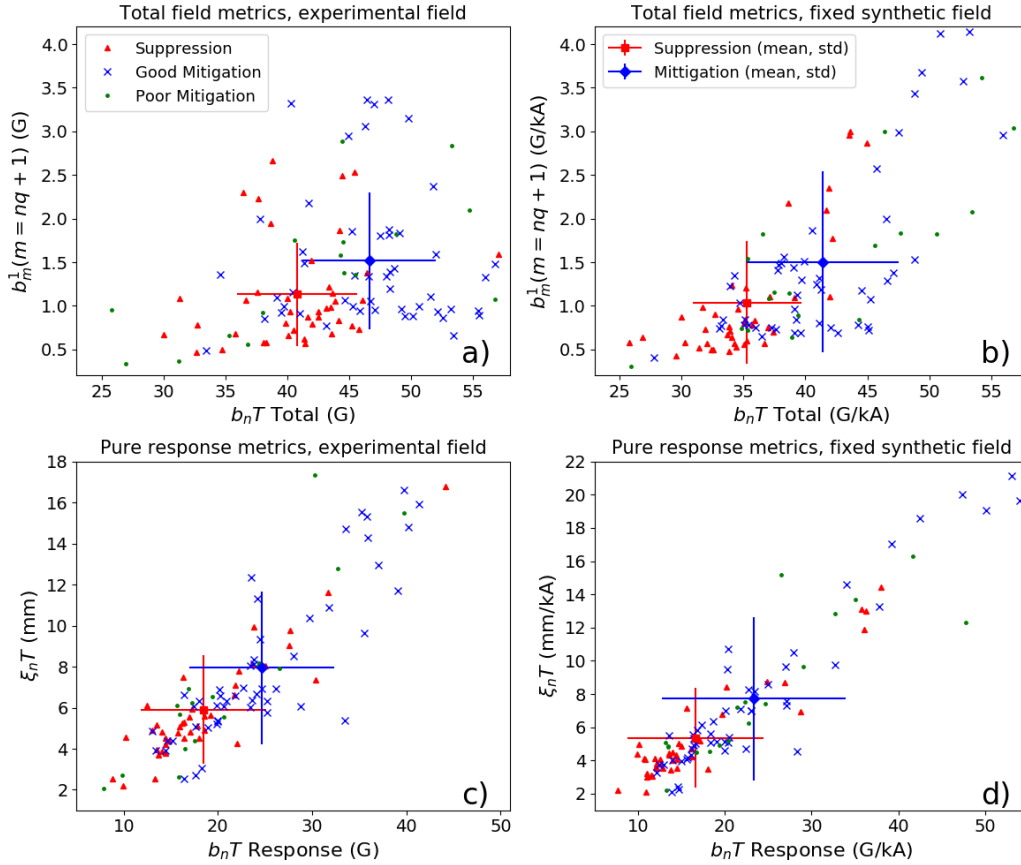
Figure 5. a) Space of plasma response metrics $b_n T_{tot}$ and $b^1_{m=nq+1}$, using experimental coil amplitude and phase, and including PSL corrections. This result represents the peeling response which occurred in experiment. b) Space of plasma response metrics $b_n T_{tot}$ and $b^1_{m=nq+1}$, using fixed coil amplitude of 5kAt and 90 degree phase, to remove applied field variation as a variable. c) Space of plasma response metrics $b_n T_{resp}$ and $\xi_n T$, using experimental coil amplitude and phase, and including PSL corrections. d) Space of plasma response metrics $b_n T_{resp}$ and $\xi_n T$, using fixed coil amplitude of 5kAt and 90 degree phase.

Figures 6a) and b) plot $b_n T_{tot}$ and $b_n T_{resp}$ against the equilibrium pedestal pressure for fixed applied field, and with triangularity restricted to $0.18 < \delta_U < 0.28$. The significant scatter in the data indicates the presence of confounding factors, and it is not possible to determine by eye whether the data exhibits a correlation between the peeling response and pedestal pressure. A linear regression analysis is performed on the two datasets to quantify and test the correlation between the peeling response and pressure pedestal. The analysis

excludes the 'poor mitigation' points, as these points are more susceptible to errors in the pressure pedestal height due to lack of ELM synchronisation. The resulting linear fits, R^2 values and Pearson correlation coefficients are plotted in figure 6. A null hypothesis that the slope of the data is zero yields a p value of 1.4×10^{-6} and 6.3×10^{-6} for the total field and pure response field respectively, which we may interpret to indicate that it is unlikely that the correlation does not exist. This result weakly supports, but does not confirm, the existence of a correlation between the peeling response and pressure pedestal in this dataset, consistent with the original hypothesis of the high triangularity requirement[2].
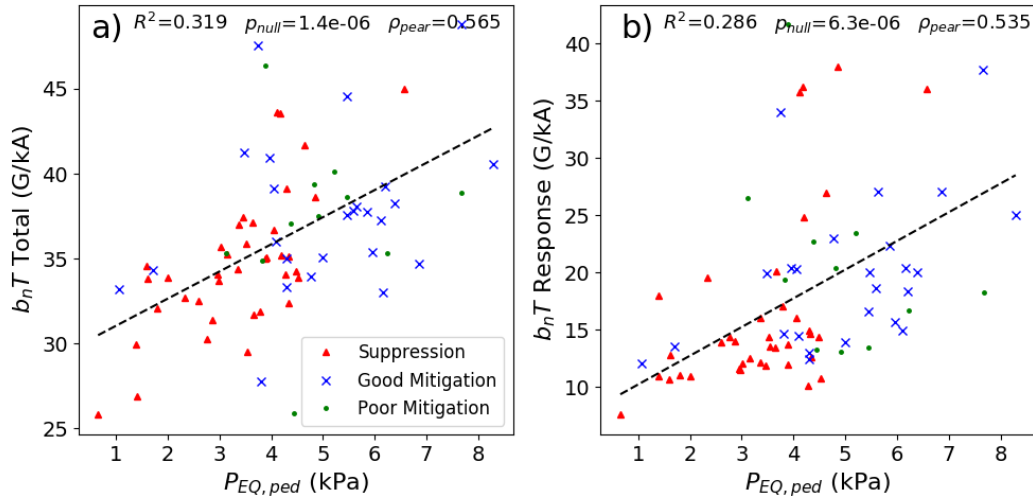
Figure 6. Plasma response metrics b_nT_{tot} and b_nT_{resp} with fixed applied field, against the pedestal pressure. Triangularity is restricted to $0.18 < \delta_U < 0.28$. Dashed lines are linear regression fits to the data. The R^2 values and Pearson correlation coefficients are annotated. The figure p_{null} is the p value of a null hypothesis that the slope of the linear fit is zero, computed to quantify the likelihood of the existence of the correlations in the plot. The p values being low in both cases, indicates that it is unlikely that the slope is zero, supporting the existence of the correlation.

Figure 7a) plots the peeling response metric b_nT_{tot} against upper triangularity δ_U. The figure shows that contrary to initial expectations, the total field including peeling response decreases strongly with δ_U. The immediate cause of this is demonstrated in figure 7c), which plots the vacuum field at the same location in the poloidal plane the b_nT_{tot} metric is measured. The figure shows that the vacuum field at the plasma top also decreases with δ_U, which causes b_nT_{tot} to be reduced accordingly. Figure 7b) plots the pure response field b_nT_{resp} against δ_U. Since the response is the amplification of the vacuum field, reduction of the vacuum field with δ_U results in a reduction of the plasma response, which is not compensated by the increasing pressure drive with increasing δ_U. Figure 7d) plots the closest distance between the upper coils and plasma boundary, against triangularity. The field applied at the coils is fixed in this plot, but the effective field which reaches the plasma strongly decreases as the gap between the coils and plasma widens, as shown in figure 7e). It appears that in practice, increasing δ_U deforms the plasma away from the coils, such that the vacuum field reaching the plasma, and

consequent plasma response, are reduced. This consequence of increasing δ_U is demonstrated in figure 8, which plots a high and low δ_U plasma boundary, and the gap between the upper and lower coils and plasma computed for the database. It is interesting to note that the effect is not confined to the upper plasma region; the gap between the plasma and lower coils also increases with δ_U. This effect dominates over the modest boost to the peeling response caused by increased pedestal pressure at high triangularity. Furthermore, referring to only the high δ_U points in figures 7a,b), it appears that for fixed triangularity the peeling response is lower in suppression than mitigation. The enhanced density pump out in suppression leading to reduced pressure drive is the suspected cause of this.
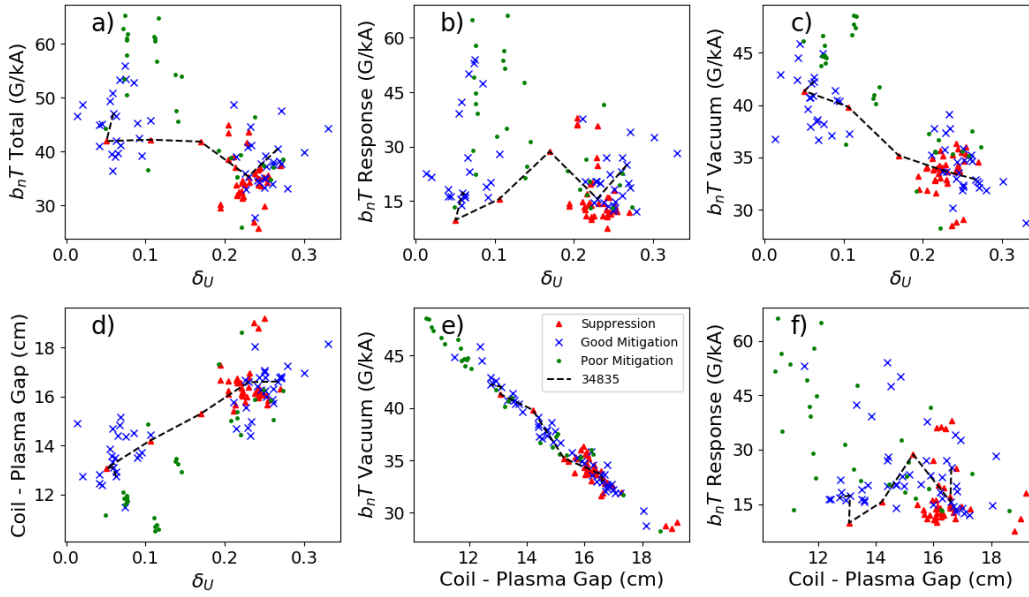
Figure 7. a) Total field metric b_nT_{tot} with fixed applied field, against δ_U. b) Pure response metric b_nT_{resp} against δ_U. c) Vacuum field at the same location as b_nT_{tot} is measured, against triangularity. d) The minimum distance from the upper coils to the plasma edge against δ_U. e) The vacuum field at the same location as the metric b_nT_{tot} is measured, against minimum distance from the coils to the plasma edge. f) Pure response metric b_nT_{resp} against the minimum distance from the upper coils to the plasma edge. In all subplots, the dashed line refers to the triangularity scan of discharge 34835.

4. Effect of triangularity on poloidal harmonic coupling mechanism

It has previously been predicted that the resonant component of the total field may be driven by the peeling response via poloidal harmonic coupling (PHC)[25]. PHC is a purely geometric effect, so it is expected to be modified by plasma shaping. In particular, coupling between modes $m \pm 1$, $m \pm 2$ and $m \pm 3$ are linked with toroidicity, elongation and triangularity respectively. The amplified peeling response typically manifests in the spectral region just above resonance with $\Delta m = 2 - 3$, where $nq = m + \Delta m$. It is therefore proposed here that increasing the triangularity may cause an increase in coupling between the resonant field and
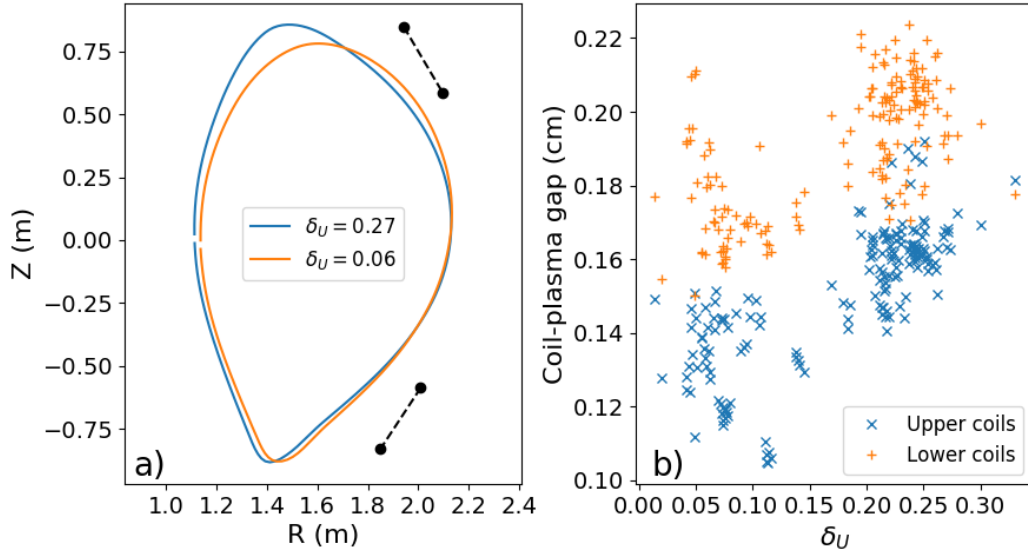
Figure 8. a) Plasma boundaries for a high and low δ_U plasma, from discharge 34835 at 2.5s and 5.6s respectively. b) Minimum gap between the upper and lower coils (coil location in (R,Z) taken to be the centre of the window coils) and the plasma boundary.

the peeling response. This could contribute to the suppression mechanism by facilitating field penetration and island formation. In this section, a scan of the plasma upper triangularity is performed, to investigate the effect of triangularity on PHC between the peeling response and the resonant field. Since PHC is a purely geometric effect, in this section for simplicity only the vacuum field is considered.

A reference shape is taken from a reconstruction of discharge 30835 at 3.2s, and the upper half of the boundary is distorted to scan the upper triangularity. The resulting plasma boundaries are plotted in figure 9a). A vacuum perturbation containing only a single poloidal harmonic m_{BC} was applied as a boundary condition at the plasma edge, as demonstrated for the highest and lowest triangularity cases in figures 9b) and 9c) respectively. The results in figures 9 and 10 use $m_{BC} = 12$, but the results were also found to be general for $m_{BC} = 10 - 16$. Figure 10 plots the amplitude of poloidal harmonics of b_m^1 at $s = 0.997$ with poloidal harmonic numbers $m_{BC}-1$, $m_{BC}-2$ and $m_{BC}-3$, normalised to the m_{BC} harmonic. The flux surface $s = 0.997$ was deliberately chosen to be very close to the plasma boundary in order to demonstrate direct $\Delta m = 1, 2, 3$ coupling with only the m_{BC} component, and reduce 'secondary' coupling between the $m = m_{BC} - 1$ and $m = m_{BC} - 2$ components. The figure shows that while the $m = m_{BC} - 1$ harmonic decreases relative to m_{BC}, the harmonics $m = m_{BC} - 2$ and $m = m_{BC} - 3$ increase with δ_U. This shows that increasing the triangularity may in principle lead to increased $\Delta m = 2, 3$ coupling between the peeling response and resonant components as proposed, but at a cost of decreased $\Delta m = 1$ coupling. The figure also shows that the $m = m_{BC} - 2$ and $m = m_{BC} - 3$ components are very small relative to the $m = m_{BC} - 1$ component (note that the $m = m_{BC} - 2$ and $m = m_{BC} - 3$ components are rescaled in the figure), indicating that toroidicity induced $\Delta m = 1$ coupling

is far stronger than the triangularity and elongation induced $\Delta m = 2, 3$ coupling.

Using the previously assembled database and fixed realistic 1kA applied RMP field, we may test whether this finding is robust to realistic fields and varying experimental boundary shapes. Figure 11a) plots $b^1_{m=nq}/b^1_{m=nq+1}$ (the ratio of the outermost vacuum resonant component to the first off-resonant component) against δ_U, while b) and c) plot the same ratio for the second and third off-resonant components. To be consistent with the results of figure 10, we would expect the ratio $b^1_{m=nq}/b^1_{m=nq+1}$ to decrease with δ_U, and the ratios $b^1_{m=nq}/b^1_{m=nq+2}$ and $b^1_{m=nq}/b^1_{m=nq+3}$ to both increase with δ_U. Instead, the plot shows that all three ratios decrease with δ_U. The field applied to the datapoints in figure 11 contains a full poloidal spectrum rather than just a single m_{BC} as in figure 10, so it is likely that the spectrum within the plasma is determined primarily by $\Delta m = 1$ coupling between directly adjacent poloidal harmonics. That is, coupling between $b^1_{m=nq}$ and $b^1_{m=nq+2}$ is driven by a chain of $\Delta m = 1$ from $b^1_{m=nq+2}$ to $b^1_{m=nq+1}$ to $b^1_{m=nq}$, rather than $\Delta m = 2$ coupling between $b^1_{m=nq+2}$ and $b^1_{m=nq}$. Figure 10 shows that the toroidicity induced $\Delta m = 1$ coupling decreases with δ_U, causing secondary coupling to $\Delta m = 2, 3$ components to be reduced in Figure 11b) and c). The reduction in toroidicity induced coupling with δ_U, dominates over the increase in elongation and triangularity induced coupling. From this we may deduce that the peeling response drive of the resonant components is weaker in high triangularity, rather than stronger as proposed at the start of this section. This result strongly contradicts the theory that increased triangularity induced PHC between the peeling response and resonant components is the cause of the triangularity requirement for suppression. It should be noted that this result does not preclude a strong resonant field being part of the suppression mechanism, it merely indicates that any resonant field present is not the result of increased PHC due to raised triangularity.
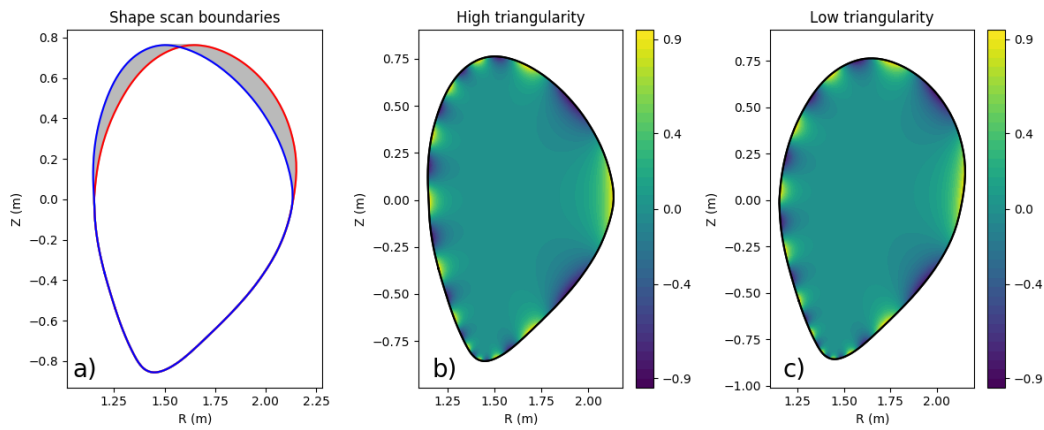
Figure 9. a) The boundary of a reference equilibrium reconstructed from discharge 30835 at 3.2s is distorted in order to scan the upper triangularity. The equilibrium is recomputed after boundary distortion using CHEASE to ensure self consistency. b,c) A single m vacuum magnetic perturbation, $m_{BC} = 12$ in the above figure, is applied to each equilibrium in the shape scan. In this figure and figure 10, the perturbation is applied as a boundary condition at the plasma edge.
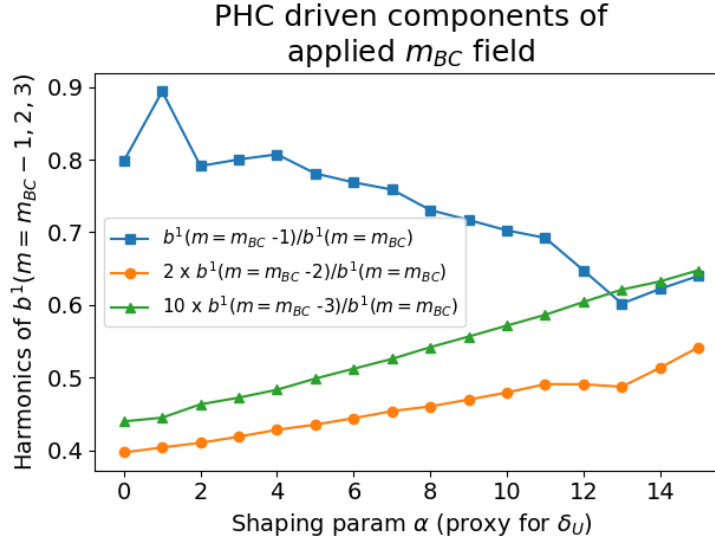
Figure 10. Harmonics with m below m_{BC}, at $s = 0.997$. These harmonics are not present in the applied field which is a pure m_{BC} field, and must be driven by PHC. Note that the $m_{BC} - 2, 3$ lines have been rescaled for conciseness. The $m_{BC} - 2, 3$ harmonics increase with δ_U, while the $m_{BC} - 1$ harmonic decreases. This indicates that elongation and triangularity induced PHC increase with δ_U, while toroidicity induced PHC decreases.
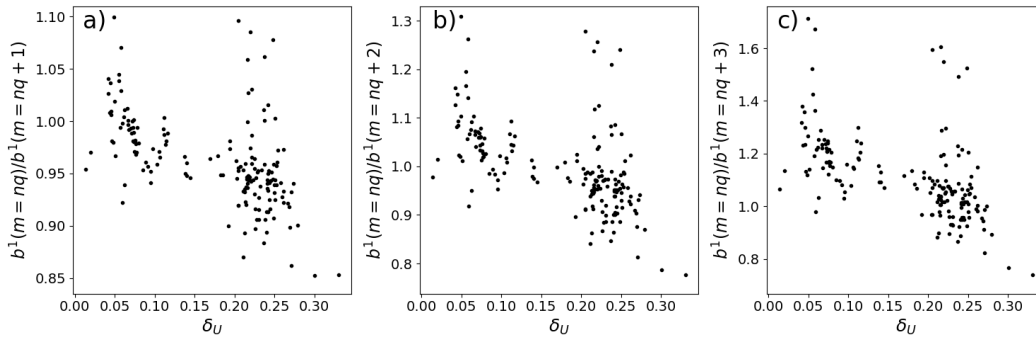
Figure 11. The outermost vacuum resonant component of a 1kA field applied at the external coils, normalised to a) the first adjacent off-resonant component $b^1_{m=nq+1}$ b) the second adjacent off-resonant component $b^1_{m=nq+2}$ c) the third adjacent off-resonant component $b^1_{m=nq+3}$. These ratios indicate the extent of coupling between the resonant components and the adjacent off-resonant components, in the spectral region occupied by the peeling response. All three ratios decrease with δ_U. This is interpreted as indicating that PHC between the resonant components and higher harmonics with $\Delta m = 1, 2, 3$, is dominated by toroidicity induced $\Delta m = 1$ coupling which is seen in figure 10 to decrease with δ_U.

5. Summary and Discussion

5.1. Initial hypothesis for high δ_U requirement

It has previously been established experimentally on ASDEX Upgrade that ELM suppression access requires good coupling between the applied field and marginally stable edge MHD modes, here called the peeling response, as well as sufficiently high upper triangularity δ_U[27]. This work is primarily concerned with testing the initial hypothesis for the requirement of high triangularity, which proposes that increasing triangularity causes an increase in the pressure pedestal, enhancing the peeling response, thereby facilitating suppression access[2]. This hypothesis implies a positive correlation between δ_U and the pedestal pressure (consistent with previous work[29]), however figure 3 shows that this is not conclusively detected in this work. The hypothesis also requires a positive correlation between pedestal pressure and peeling response, which is shown in figure 6 to be likely to exist, although the peeling response is only very weakly sensitive to the pedestal pressure. Contrary to expectation, it is demonstrated in figure 7 that since creating the high triangularity plasma shape necessitates moving the plasma edge away from the RMP coils, the resultant reduction in effective vacuum field causes a net decrease in the peeling response with triangularity. Therefore, the requirement of high δ_U for suppression is not due to the requirement of an enhanced peeling response, as was supposed[2].

5.2. Poloidal harmonic coupling hypothesis for high δ_U requirement

An alternative explanation for the high triangularity requirement is proposed here, that increasing the triangularity may increase $\Delta m = 3$ poloidal harmonic coupling, allowing the peeling response to more strongly drive the resonant components for a fixed peeling response, facilitating field penetration. It is demonstrated in figure 10 that $\Delta m = 3$ poloidal harmonic coupling does increase with triangularity as expected. However despite this, it is shown in figure 11 that coupling between the $m = nq$ and $m = nq + 3$ components in fact decreases with triangularity due to decreasing toroidicity induced coupling, so this hypothesis is also rejected. Another explanation for the requirement of high triangularity is therefore required.

5.3. Alternative hypothesis for future work

5.3.1. Pertinent observations The hypothesis explained below builds on that in [16], and relies on the following observations from experiment and simulation:

(1) Corrugation of the plasma edge degrades P-B stability[16, 17, 18].
(2) During ELM mitigation, corrugation of the plasma edge correlates with density pump-out[36, 26] (although this correlation may not hold in suppression as discussed below).

(3) The peeling response amplifies plasma edge corrugation[12].

(4) During ELM mitigation, the peeling response correlates with mitigated ELM frequency[26, 41].

(5) Suppression access requires density to be reduced below some threshold[27].

(6) Suppression access requires the peeling response to exceed some threshold[27].

We add to this list, the following two results from this present work.

5.3.2. Possible breaking of correlation between peeling response and density pump out in suppressed phase. It is observed that the suppression transition is accompanied by an enhanced density pump out [27]. This work finds that in contrast to the mitigated phase, the enhanced pump out in suppression has no accompanying increase in the peeling response, implying that the correlation between density pump out and edge corrugation does not hold for suppression. This is consistent with experimental observations on the EAST tokamak[8], in which the coil current was ramped linearly in time, and the density decreased due to RMP induced pump out. Once the suppression density threshold was reached and suppression accessed, the density suddenly dropped further, and then remained constant even as the coil current continued to increase. This demonstrated that the correlation between the peeling response (which increases linearly with coil current) and density pump out had been broken at the suppression transition. This suggests that the mechanism of the enhanced density pump out in the suppressed phase, is distinct from the mechanism for density pump out in the mitigated phase, as previously suggested in [42]. This may be related to an observation on DIII-D, of an increase in long wavelength electron temperature turbulence during the RMP ELM suppressed phase relative to the RMP mitigated phase[43].

5.3.3. Possible breaking of correlation between pedestal pressure and δ_U by application of RMPs. Failure to confirm the expected correlation between the pedestal pressure and δ_U in figure 3, may simply mean that the correlation was disrupted by confounding variables in this study, however there is a more interesting interpretation. With the coils off, ELM crashes determine the pedestal limit, so we expect high and low δ_U points to sit on their respective P-B boundaries, allowing high triangularity plasmas to achieve larger values of (j, α). This is why we expect the correlation to exist. However, with the RMP coils active, the RMP induced confinement degradation (evidenced by density pump out) determines the pedestal limit, so the dependence of the pedestal gradient on δ_U may be significantly weakened or broken. If this were true, we may expect the high and low δ_U operational points to occupy similar regions of (j, α) space with the RMP coils on, but with the RMP coils off the high δ_U operational points should have higher (j, α) values than low δ_U points. Figure 12b) and c) plot the points of the database in (j, α) space, distinguishing between high and low δ_U points and mitigation and suppression points. The large overlap of the regions occupied by the high and low triangularity points in figure b) is consistent with our supposition that with coils active, the

dependence of the pedestal gradient limit on δ_U is weakened or broken. Unfortunately since there are no "RMP off" operational points in the database, this remains merely a supposition awaiting future study.

5.3.4. Proposed physical mechanism of the high δ_U requirement. Bearing in mind the diverse observations explained above, consider now an increasing ramp of the peeling response, which may be achieved either by ramping the RMP coil current, or by tuning the applied field using the phase difference between the upper and lower coil sets. As the peeling response increases, the operational point will move towards lower regions of (j, α) space (by observations 2) and 3)), as will the P-B stability boundary (by observations 1), 3) and 4)). We may now use observations 2), 3) and 5) to postulate an explanation for observation 6). Ie, it is proposed that the reason a large peeling response is required, is that the peeling response must be large enough to drive sufficient density pump-out to reduce the plasma density below the suppression access threshold. Furthermore, it is conceivable that in the process of exceeding the required peeling response threshold for suppression access, the P-B stability may become so degraded that the stability boundary catches up with the operational point in (j, α) space, which would keep the pedestal unstable and preclude suppression. For the low δ_U points, movement of the boundary with increasing corrugation is more likely to overtake the operational point, keeping the operational point P-B unstable. Conversely the operational points for the high δ_U cases are further from the P-B boundary, and therefore more resilient to corrugation induced destabilisation. The above picture is sketched in figure 12a), and may provide a basis for explaining why increasing the triangularity facilitates suppression access. To summarise, it is supposed that the mitigation mechanism may preclude suppression access, and this scenario is more likely in low than high triangularity, which would explain the requirement for high triangularity. An observed correlation between the peeling response and the reappearance of ELMs in suppressed phases reported in [44], supports the supposition that the mitigation mechanism may preclude suppression. This work finds that the observed increase in density pump out which occurs at the transition to suppression is not accompanied by an increase in the peeling response. This suggests that at the suppression transition the operational point is moved further into the stable (j, α) region, but because the corrugation does not increase, the stability boundary remains at its pre-transition location. This would increase the distance of the operational point from the stability boundary after the transition, and is consistent with the observation that the conditions to maintain suppression are less stringent than for suppression access[27].

5.4. Assumptions and limitations

5.4.1. Incomplete evidence base Firstly, the above hypothesis requires the supposition that the correlation between δ_U and pedestal pressure is broken or critically weakened by the application of RMPs, so that the high and low δ_U points occupy the same region of (j, α)

space, whereas with the RMPs off they would be found at their respective P-B boundaries. Evidence for this supposition is currently very weak, since there are no RMP off points in the database. Secondly, the hypothesis makes use of the observation of a density threshold for suppression access, but makes no attempt to explain it. Thirdly, the above hypothesis also requires the supposition that since unperturbed high δ_U equilibria have greater stability than low δ_U equilibria, then perturbed high δ_U equilibria will have enhanced stability relative to perturbed low δ_U equilibria. To test this hypothesis, models must be developed capable of mapping the P-B linear stability space of highly shaped experimental 3D equilibria including rotation, and the stability maps of high and low δ_U 3D equilibria compared. Several such models have been developed[45], or are near completion[46, 47, 48].

5.4.2. Exclusion of non-linear processes Recent works indicate that the transition to suppression is a non-linear bifurcation process, involving a rapid penetration of the resonant field and the formation of one or more magnetic islands[8, 21]. With only linear physics as in the above picture, the suppression transition itself cannot be understood. By focussing on only established and slowly varying suppressed or mitigated phases as in this study, the problem of treating the non-linear transition is bypassed, and the suppressed state may be studied with only linear models. Furthermore, the single fluid model used in this study is unsuitable to describe the screening physics accurately, and therefore may not distinguish between the penetrated state which features islands, and the screened state. A two-fluid model as employed in [49] would be more appropriate. This study therefore focusses on the amplified peeling response rather than the resonant response. It is not considered necessary to know the resonant response accurately to compute the peeling response, since although there is evidence that the peeling response can drive the resonant components[25, 50], there is currently no evidence of a causal relation in the opposite direction. This is consistent with agreement between resistive and ideal MHD codes (MARS-F and VMEC) on predictions of the peeling response[13]. The destabilisation due to 3D effects is driven by plasma surface corrugation, which is driven by the peeling response rather than the resonant response[16], so it is not expected that a penetrated plasma would have significantly different stability properties to an otherwise identical screened plasma. A strong resonant response would of course modify the rotation braking and edge transport properties, but the effects of these modifications manifest in the rotation and kinetic profiles, which can be measured and used as input to a linear model. Therefore a linear stability code which includes physics effects relevant to the P-B stability boundary (most notably, 3D corrugation and rotation) should be able to predict the stability of a suppressed penetrated plasma state even without knowledge of the bifurcation process by which it arrived at that state. Therefore the non-linear transition process described in [21] does not preclude the suppressed state being understood using linear response and stability models as proposed above.
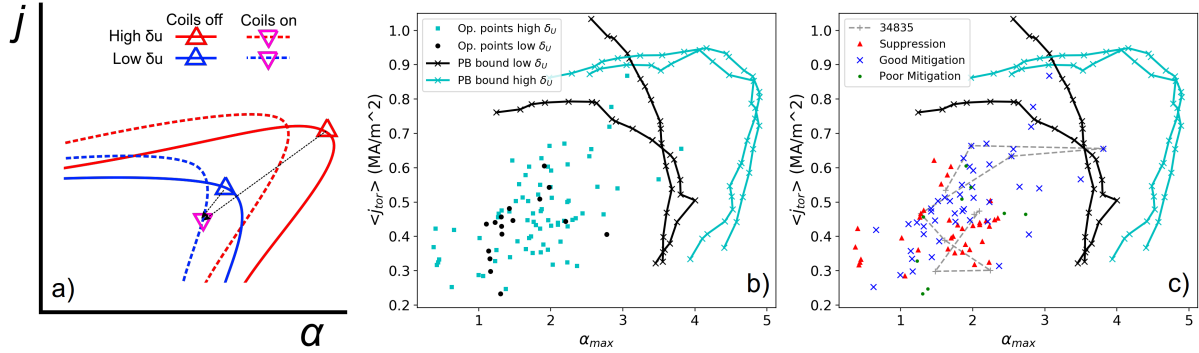
Figure 12. Sketch of the alternative explanation of high triangularity requirement. a) As explained in [16], with increasing peeling response the density pump out moves the experimental point towards stability, while corrugation lowers the stability boundary. In low triangularity, it is suggested here that the boundary moves such that the experimental point remains always in the unstable region, whereas in high triangularity, the enhanced stability allows the experimental point to enter the stable region for some values of the peeling response. b) The operational points in (j, α) space for the database are plotted for high and low triangularity. Using the MISHKA code[51], finite-n peeling ballooning stability boundaries are computed for two representative high and low δ_U points from the database, demonstrating that the peeling-ballooning stability is significantly enhanced by increased shaping as expected[29]. The approximate co-location of the high and low δ_U points suggests that the dependence of (j, α) on δ_U is weakened or broken by RMP induced confinement degradation. The distance from the operational points to the stability boundaries is therefore larger in the high δ_U case, making these points more resilient to movement of the boundary by corrugation. c) The operational points in (j, α) space for the database are plotted for suppression and mitigation points. It should be noted that the (j, α) points in b) and c) are derived from equilibria produced by CLISTE, rather than by HELENA as is conventional for these plots[52]. However it has been shown that the edge current density of kinetically constrained CLISTE equilibria are in good agreement with predictions of neoclassical currents[53]. It should also be noted that ELM synchronisation was not performed, so the plotted values of (j, α) for the mitigated plasmas as slightly below their values immediately preceding an ELM crash.

Acknowledgements

References

[1] H Meyer *et al*, 2017, *Nuclear Fusion*, **57**, 102014.

[2] R Nazikian *et al*. First Observation of ELM Suppression by Magnetic Perturbations in ASDEX Upgrade and Comparison to DIII-D Matched-Shape Plasmas. In *26th IAEA Int. Conf. on Fusion Energy*, 1–8, Kyoto, Japan, 2016.

[3] N Oyama, 2008, *Journal of Physics: Conference Series*, **123**, 012002.
[4] A Loarte *et al*, 2003, *Plasma Physics and Controlled Fusion*, **45**, 1549–1569.
[5] T E Evans *et al*, 2004, *Physical Review Letters*, **92**, 235003.
[6] W Suttrop *et al*, 2018, *Nuclear Fusion*, **58**, 096031.
[7] Y M Jeon *et al*, 2012, *Physical Review Letters*, **109**, 035004.
[8] Y Sun *et al*, 2016, *Physical Review Letters*, **117**, 115001.
[9] A Kirk *et al*, 2013, *Plasma Physics and Controlled Fusion*, **55**, 124003.
[10] W Suttrop *et al*, 2011, *Physical Review Letters*, **106**, 225004.
[11] P R Thomas, 2008, *Proc. 22nd Int. Conf. on Fusion Energy 2008*.
[12] M Willensdorfer *et al*, 2017, *Nuclear Fusion*, **57**, 116047.
[13] M Willensdorfer *et al*, 2016, *Plasma Physics and Controlled Fusion*, **58**, 114004.
[14] I T Chapman *et al*, 2014, *Nuclear Fusion*, **54**, 083006.
[15] A Kirk *et al*, 2012, *Physical Review Letters*, **108**, 255003.
[16] I T Chapman *et al*, 2013, *Physics of Plasmas*, **20**, 056101.
[17] C J Ham *et al*, 2014, *Physics of Plasmas*, **21**, 102501.
[18] M Willensdorfer *et al*, 2017, *Physical Review Letters*, **119**, 085002.
[19] A Kirk *et al*, 2013, *Nuclear Fusion*, **53**, 043007.
[20] M.R. Wade *et al*, 2015, *Nuclear Fusion*, **55**, 023002.
[21] R Nazikian *et al*, 2015, *Physical Review Letters*, **114**, 105002.
[22] Y Liu *et al*, 2010, *Physics of Plasmas*, **17**, 122502.
[23] M J Lanctot *et al*, 2013, *Nuclear Fusion*, **53**, 083019.
[24] S R Haskey *et al*, 2014, *Plasma Physics and Controlled Fusion*, **56**, 035005.
[25] D A Ryan *et al*, 2015, *Plasma Physics and Controlled Fusion*, **57**, 095008.
[26] D A Ryan *et al*, 2018, *Plasma Physics and Controlled Fusion*, **60**, 065005.
[27] W Suttrop *et al*, 2017, *Plasma Physics and Controlled Fusion*, **59**, 014049.
[28] R J Groebner *et al*, 1998, *Plasma Physics and Controlled Fusion*, **40**, 673–677.
[29] F M Laggner *et al*, 2018, *Nuclear Fusion*, **58**, 046008.
[30] E. Viezzer *et al*, 2012, *Review of Scientific Instruments*, **83**, 103501.
[31] P J Mc Carthy, 2012, *Plasma Physics and Controlled Fusion*, **54**, 015010.
[32] W Suttrop *et al*. Physical description of external circuitry for Resistive Wall Mode control in ASDEX Upgrade. In *36th EPS Conference on Plasma Physics*, volume 33 E1, 458–461, 2009.
[33] J D King *et al*, 2015, *Physics of Plasmas*, **22**, 072501.
[34] P Piovesan *et al*, 2017, *Plasma Physics and Controlled Fusion*, **59**, 014027.
[35] Y Liu *et al*, 2000, *Physics of Plasmas*, **7**, 3681.
[36] Y Liu *et al*, 2011, *Nuclear Fusion*, **51**, 083002.
[37] D A Ryan *et al*, 2017, *Plasma Physics and Controlled Fusion*, **59**, 024005.
[38] D. J. Ward *et al*, 1995, *Physics of Plasmas*, **2**, 1570.
[39] L Li *et al*, 2017, *Plasma Physics and Controlled Fusion*, **59**, 044005.
[40] Y Liu *et al*, 2016, *Nuclear Fusion*, **56**, 056015.
[41] A Kirk *et al*, 2015, *Nuclear Fusion*, **55**, 043011.
[42] S. Mordijck *et al*, 2011, *Plasma Physics and Controlled Fusion*, **53**, 122001.
[43] C. Sung *et al*, 2017, *Physics of Plasmas*, **24**, 112305.
[44] A Wingen *et al*, 2015, *Plasma Physics and Controlled Fusion*, **57**, 104006.
[45] T Weyens *et al*, 2017, *Journal of Computational Physics*, **330**, 997–1009.
[46] M S Anastopoulos-Tzanis *et al*. Perturbative 3D Ideal MHD Stability of Tokamak Plasmas. In *45th EPS Conference on Plasma Physics*, 1–4, Prague, 2018.
[47] E Strumberger *et al*, 2017, *Nuclear Fusion*, **57**, 016032.
[48] C Nührenberg, 2016, *Nuclear Fusion*, **56**, 076010.
[49] S. Mordijck *et al*, 2014, *Nuclear Fusion*, **54**, 082003.
[50] F Orain *et al*, 2017, *Nuclear Fusion*, **57**, 022013.
[51] A B. Mikhailovskii *et al*, 1997, *Plasma Physics Reports*, **23**, 844–857.

[52] S Saarelma *et al*, 2013, *Nuclear Fusion*, **53**, 123012.

[53] M G Dunne *et al*, 2012, *Nuclear Fusion*, **52**, 123014.